Shape Analysis of the Femoral Head: A Comparative Study Between Spherical, (Super)Ellipsoidal, and (Super)Ovoidal Shapes

Daniel Simões Lopes[1]
Visualization and Intelligent Multimodal Interfaces Group,
INESC ID Lisboa,
Rua Alves Redol, 9,
Lisbon 1000-029, Portugal
e-mail: daniel.lopes@inesc-id.pt

Richard R. Neptune
Mem. ASME
Department of Mechanical Engineering,
The University of Texas at Austin,
Austin, TX 78712
e-mail: rneptune@mail.utexas.edu

Artur A. Gonçalves
Instituto Superior Técnico,
Universidade de Lisboa,
Avenida Rovisco Pais 1,
Lisbon 1049-001, Portugal
e-mail: artur.goncalves@tecnico.ulisboa.pt

Jorge A. Ambrósio
Instituto Superior Técnico,
Universidade de Lisboa,
Avenida Rovisco Pais 1,
Lisbon 1049-001, Portugal
e-mail: jorge@dem.ist.utl.pt

Miguel T. Silva
Instituto Superior Técnico,
Universidade de Lisboa,
Avenida Rovisco Pais 1,
Lisbon 1049-001, Portugal
e-mail: MiguelSilva@ist.utl.pt

In this work, MacConaill's classification that the articular surface of the femoral head is better represented by ovoidal shapes rather than purely spherical shapes is computationally tested. To test MacConaill's classification, a surface fitting framework was developed to fit spheres, ellipsoids, superellipsoids, ovoids, and superovoids to computed tomography (CT) data of the femoral proximal epiphysis. The framework includes several image processing and computational geometry techniques, such as active contour segmentation and mesh smoothing, where implicit surface fitting is performed with genetic algorithms. By comparing the surface fitting error statistics, the results indicate that (super)ovoids fit femoral articular surfaces better than spherical or (super)ellipsoidal shapes. [DOI: 10.1115/1.4031650]

Keywords: femoral head, implicit surfaces, (super)ellipsoids, (super)ovoids, least-square minimization, surface fitting

1 Introduction

For spheroidal articular surfaces, such as the humeral and femoral heads, the standard classification regarding shape modeling is that these surfaces can be represented by spherical shapes [1–3]. Despite this classification, several authors within the orthopedic surgery and prosthetic design communities have noted that the femoral head and acetabular cavity are not clearly spherical, but are actually more complex in shape exhibiting quasi-homogeneous curvatures [4–16]. Most of these studies use spheres and ellipsoids to describe the shapes [4–11], although some consider conchoids [4,7,15].

Contrary to these shape classifications, MacConaill and coworker provided a series of anatomical observations which led to a more complex classification based on joint morphology: spheroidal articular surfaces such as the femoral head are better represented by ovoidal (i.e., egglike) forms rather than spherical since a sphere does not account for more global characteristics such as axial asymmetry and nonhomogeneous curvature [17–19]. However, there have not been computational studies to test MacConaill's ovoidal classification regarding the femoral head. Thus, by using surface fitting tools that consider ovoidal shapes as geometric primitives, it is expected that ovoidal shapes will provide better approximations of the global characteristics of the femoral head and, consequently, will lead to a better understanding and treatment of many degenerative joint diseases [4], reduce the overall time of the surgical operation, and inspire new joint prosthetic designs [7,17–19].

Therefore, the objective of this study was to perform a shape analysis of the femoral head in order to computationally test MacConaill's ovoidal joint classification. To this end, a computational framework for fitting implicit surface models was developed using spheres, (super)ellipsoids [20], and (super)ovoids [21] as the geometric primitives to describe the articular surfaces. The implicit surface fitting tool extracts global aspects that reflect joint morphology of spheroidal articular surfaces from CT data sets of the hip region. A comparative study was then performed between the geometric primitives to identify which primitive provides a more precise mathematical description of the morphofunctional aspects of the spheroidal articular surface. The surface fitting framework uses genetic algorithms to solve a least-square minimization problem to compare how well the geometric primitives approximate the anatomical data from the CT images. Thus, the higher the goodness-of-fit the better a geometric primitive describes, macroscopically, the articular surface of a femoral head. It should be noted that the suitability of ovoidal shapes to represent the femoral head has been provided by MacConaill and coworker [17–19]. However, no study has used a computational approach to fit a superellipsoid or (super)ovoid to the femoral articular surface to explicitly test the MacConaill classification.

2 Methodology

2.1 Geometric Primitives or Shape Models. The considered shape models are idealized geometries with geometric characteristics that match macroscopic features of spheroidal articular surfaces such as: convexity, C^2 continuity, spherelike topology, and their ability to represent limited and closed surfaces. In the case of superellipsoids, they consist of a generalization of spherical and ellipsoidal surfaces proposed by Barr [20] by replacing the fixed exponent by an arbitrary non-negative number equal to or larger than 2. In the case of superovoids, they consist of a generalization of an ovoidal form proposed by Todd and Smart [21] after replacing the fixed quadratic exponent by an arbitrary non-negative number greater than 2. The implicit surface expressions for a superellipsoid (F_{SQ}) and superovoid (F_{SO}) in the canonical form are written as

$$F_{\mathrm{SQ}}(x_l, y_l, z_l) = 1 \Longleftrightarrow x_l^{\gamma_1} + y_l^{\gamma_2} + z_l^{\gamma_3} = 1 \quad (1)$$

[1]Corresponding author.

Manuscript received April 10, 2015; final manuscript received September 13, 2015; published online October 1, 2015. Assoc. Editor: Tammy L. Haut Donahue.

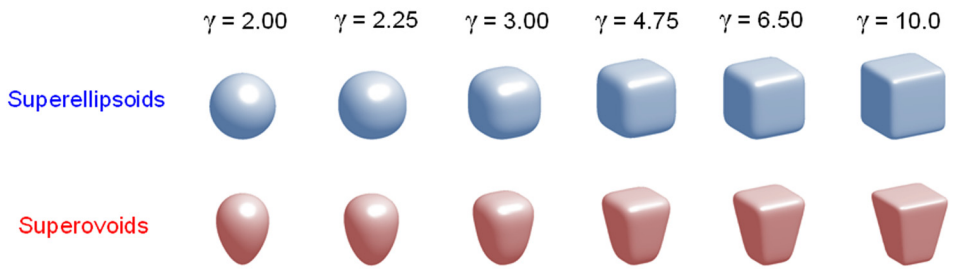

Fig. 1 Unit-sized superellipsoids and superovoids for varying exponent values

$$F_{SO}(x_l, y_l, z_l) = 1 \Longleftrightarrow \frac{x_l^{\gamma_1}}{\left(c_{0x} + c_{1x}z_l + c_{2x}z_l^2 + c_{3x}z_l^3\right)^{\gamma_1}} + \frac{y_l^{\gamma_2}}{\left(c_{0y} + c_{1y}z_l + c_{2y}z_l^2 + c_{3y}z_l^3\right)^{\gamma_2}} + z_l^{\gamma_3} = 1 \quad (2)$$

where x_l, y_l, and $z_l \in \mathbb{R}$ are the local coordinates of the point in space that belongs to the surface; γ_1, γ_2, and $\gamma_3 \in \mathbb{R}^+ \backslash \{0\}$ are real non-negative exponents; and c_{0x}, c_{1x}, c_{2x}, c_{3x}, c_{0y}, c_{1y}, c_{2y}, and c_{3y} are the ovoidal shape coefficients.

The values of γ_1, γ_2, and γ_3 are bounded between 2 and less than infinity so that only smooth convex shapes are modeled. The ovoidal shape coefficients are bounded between $0 \leq c_{0x}, c_{1x}, c_{0y}, c_{1y} \leq 1$ and $-0.1 \leq c_{2x}, c_{3x}, c_{2y}, c_{3y} \leq 0.1$. By varying the exponent values, the surface shape is mediated between spherical and rectangular shapes (Fig. 1).

Affine transformations are applied to the unit shape model, described by Eqs. (1) and (2), by converting local coordinates, $\mathbf{x}_l$, to global coordinates, $\mathbf{x}_g$, by an affine matrix transformation that incorporates a scaling matrix, $\mathbf{D}$, that contains shape coefficients and dimension parameters (e.g., in millimeters) a, b, and c along the x_l, y_l, and z_l directions, a rotation matrix, $\mathbf{R}$, and a translation column vector, $\mathbf{t}$, as

$$\mathbf{x}_l = \begin{bmatrix} x_l & y_l & z_l & 1 \end{bmatrix}^{\mathrm{T}} = \left(\left[\begin{array}{c|c} \mathbf{RD} & \mathbf{t} \\ \hline \mathbf{0}_{1\times 3} & 1 \end{array} \right] \right)^{-1} \mathbf{x}_g \quad (3)$$

where $\mathbf{x}_l$ and $\mathbf{x}_g$ are written in homogeneous coordinates.

2.2 Three-Dimensional Reconstruction of Articular Surfaces of Synovial Joints. In order to computationally test the ovoidal classification on spheroidal articular surfaces, a computational framework was developed (Fig. 2) [22–25]. The framework takes as input a collection of CT image data sets of the hip region free from considerable noise or artifacts [26]. None of the subjects scanned revealed a visible hip joint pathology. The image spatial resolution was close to 10^{-1} mm^3, which reveals both global and local details. Hip image sets of 11 subjects with ages between 21 and 39 yr (27.5 ± 5.6 years, 5 males and 6 females) were analyzed: Ten multidetector CT scans of the entire pelvis and both femurs (512 × 512 acquisition matrix, in-plane x and y resolutions = 0.2155–0.2637 mm, slice thickness = 0.70–1.0 mm, and 241–357 slices) are available from the Musculoskeletal Research Laboratories at the University of Utah.[2] In addition, a single hip image set (512 × 512 acquisition matrix, in-plane resolution = 0.664 × 0.664 mm, slice thickness = 1.5 mm, and 356 slices) was scanned using a Philips MX 8000 IDT 16 (Philips Medical Systems, Eindhoven, The Netherlands) and can be found in OsiriX's DICOM sample image sets website (the PELVIX case [27]).[3] Consent for the use of the CT data sets was provided by the subjects.

After applying a global threshold to the images, the bone regions were segmented with 3D active contours and all segmentation errors were manually corrected. Three-dimensional triangular surface meshes of the femoral heads are generated from the segmented data with a marching cubes algorithm [28]. Since this mesh presents undesired scanning features, primarily a zigzagged artifact, mesh filtering was carried out with a Laplacian filter. From the reconstructed 3D meshes, the articular surfaces were manually delimited based on anatomical knowledge of bone topography by identifying smooth regions exhibiting closely homogenous curvature. After deleting the edges and faces of this triangular mesh, the mesh vertices were then converted to a point cloud. Since the obtained point clouds are dense (on the order of tens of thousands of points), only a few thousand points are needed for surface fitting. Thus, Gaussian sampling [29], which is a down sampling procedure, is performed so that a homogeneous and representative set of points is obtained for the femoral articular surfaces (1216.7 ± 219.4 points). For a more detailed description of the framework for 3D reconstruction of anatomical structures, see Refs. [30,31].

2.3 Surface Fitting With Genetic Algorithms and Error Analyses. Fitting an implicit surface to a cloud of points was formalized as a nonlinear optimization problem with simple boundary constraints [7] as follows: given a set of N points in Cartesian space, $\mathrm{P} = \{\mathbf{x}_i : \mathbf{x}_i \in \mathbb{R}^3, i = 1,\ldots,N\}, N \in \mathbb{N}$, which belongs to the outer cortical bone surface of spheroidal joints, determine the vector of geometric parameters, $\boldsymbol{\lambda} \in \mathbb{R}^M$, where $M \in \mathbb{N}$ is the number of geometric modeling parameters (Table 1) that minimizes the error-of-fit objective function, EOF($\boldsymbol{\lambda}$), defined as the square sum of residuals (f), where each residual is the difference between the shape model function and the corresponding point datum as

$$\min_{\boldsymbol{\lambda}} \mathrm{EOF}(\boldsymbol{\lambda}) = \min_{\boldsymbol{\lambda}} \sum_{i=1}^{N} f_i^2(x_g, y_g, z_g; \boldsymbol{\lambda}) = \min_{\boldsymbol{\lambda}} \sum_{i=1}^{N} \left(1 - F_i(x_g, y_g, z_g; \boldsymbol{\lambda})\right)^2 \quad (4)$$

subjected to

$$\mathbf{l} \leq \boldsymbol{\lambda} \leq \mathbf{u} \quad (5)$$

where $\mathbf{l}$, $\mathbf{u} \in \mathbb{R}^M$ are lower and upper bound column vectors, respectively, that delimit the admissible set of the solution space, and F is the implicit surface representation presented by Eqs. (1) and (2). Note that vector $\boldsymbol{\lambda}$ contains the global anatomical information which includes the rotation and translation parameters used in the affine transformations, curvature, and asymmetry, where the latter applies only for ovoids.

The admissible set, $\Omega \subseteq \mathbb{R}^M$, or surface parameter space can be expressed as the following compact set (i.e., limited and closed set hypercube):

[2] http://mrl.sci.utah.edu/software/hip-data/
[3] http://www.osirix-viewer.com/datasets/

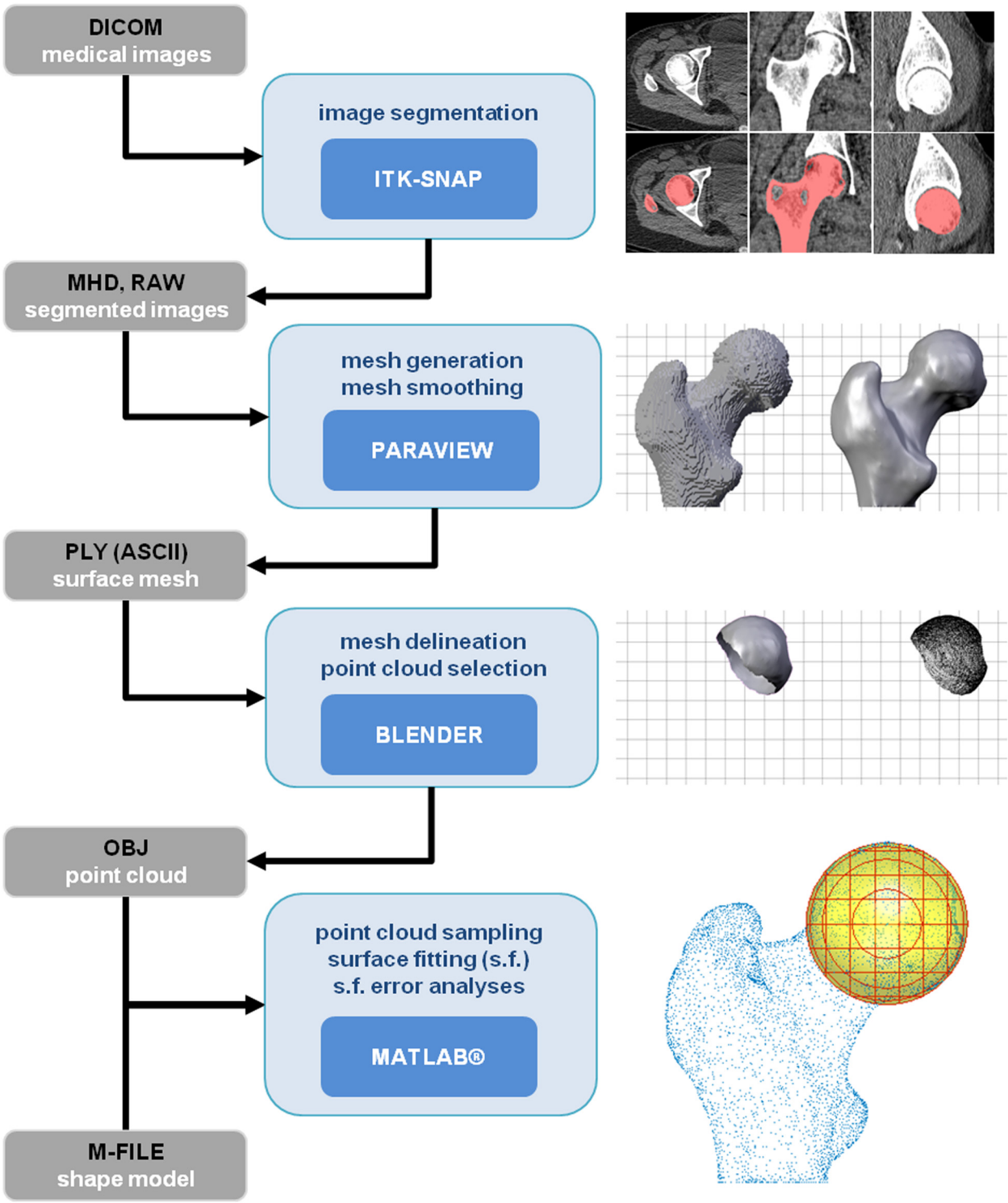

Fig. 2 Computational framework for information extraction and geometric modeling of spheroidal articular surfaces. An implicit shape model is fitted to medical image data, thus providing quantitative information regarding global geometric characteristics. File formats and software tools are shown. The software versions used are ITK-SNAP 2.2.0, PARAVIEW 3.10.1, BLENDER 2.43, and MATLAB® R2009b.

$$\boldsymbol{\lambda} \in \Omega = \bigcup_{k=1}^{M} I_k = [a_0, a_1] \times [b_0, b_1] \times [c_0, c_1] \times \ldots \times [\phi_0, \phi_1] \times [\theta_0, \theta_1] \times [\psi_0, \psi_1] \subseteq \mathbb{R}^M \quad (6)$$

where I_k is a real-valued interval of the kth surface parameter, {0,1} subscript indices designate the start and end value of the kth interval, and $M = 9,12,17,20$ is the total number of surface parameters for the ellipsoid, superellipsoid, ovoid, and superovoid models, respectively. As for spheroidal surfaces, the shape parameters must be constrained, where the values for a, b, and c are all positive, and γ_1, γ_2, and γ_3 are confined to be greater than or equal to 2 and lesser than infinity. The nonlinearity of each objective function and the presence of a large number of local minima require

the use of metaheuristic methods, such as genetic algorithms, to numerically solve the minimization problem. The Genetic Algorithm and Direct Search Toolbox™ from MATLAB® is used for implementing the surface fitting code running on an Intel® Core 2 Duo processor 1.66 GHz and 2 GB of RAM.

To calculate the surface fitting error to compare the goodness-of-fit between the different geometric primitives, it is necessary to calculate the minimum Euclidean distances from each point of the point cloud to the fitted surface. Note that the residual value f defined by Eq. (4) is not equal to the physical distance except for the spherical case, hence it is a pseudo-Euclidean distance. Unfortunately, the exact geometric distance from a point to an arbitrary (super)ellipsoid or (super)ovoid surface cannot be expressed analytically. Here, the minimum distance between each point of the point cloud and the optimally fitted geometric primitive is calculated by taking the signed Euclidean distance, $\mathrm{SED}(\mathbf{x}_Q)$, as

$$\min_{\mathbf{x}_Q} \mathrm{SED}(\mathbf{x}_Q;\mathbf{x}_P) = \min_{\mathbf{x}_Q} \mathrm{sign}(F(\mathbf{x}_P))\|\mathbf{x}_P - \mathbf{x}_Q\|_2 = \min_{\mathbf{x}_Q} \|\mathbf{d}_{PQ}\|_2 \tag{7}$$

subjected to the nonlinear equality constraint

$$F(\mathbf{x}_Q;\boldsymbol{\lambda}^*) = 1 \tag{8}$$

with $\mathbf{x}_Q$ being contained in the vicinity of $\mathbf{x}_P$

$$\mathbf{x}_P - \boldsymbol{\varepsilon} \le \mathbf{x}_Q \le \mathbf{x}_P + \boldsymbol{\varepsilon} \tag{9}$$

where $\mathbf{x}_Q \in \mathbb{R}^3$ is the surface point with minimum distance, $\mathbf{x}_P \in$ P is the given point from the point cloud, which can be inside, outside, or upon the fitted surface, $\mathbf{d}_{PQ} \in \mathbb{R}^3$ is the distance vector between the given point P and the iterated point Q, F is the implicit surface representation given by Eqs. (1) and (2), sign(.) is the sign function, $\boldsymbol{\lambda}^*$ is the vector of geometric parameters of the optimally fitted surface, and $\boldsymbol{\varepsilon}$ is a tolerance vector (e.g., $\boldsymbol{\varepsilon} = \varepsilon[1\ 1\ 1]^T$). Here, ε is considered to be much smaller comparatively to the axial dimensions of the surface, $\varepsilon = 3.0$ mm. In this case, the admissible set is given by the set of points contained in a cubic box, 2ε wide, and that satisfies the nonlinear equality constraint defined by the zero-set implicit surface functions of Eqs. (1) and (2). The same genetic algorithm code (MATLAB® optimization toolbox) was used to solve this optimization problem.

The CT images of the five male and six female normal hip joints were considered to analyze the shape of the femoral head. The goodness-of-fit was determined by measuring the surface fitting errors or, in other words, the signed Euclidean distance between the scanned points and the idealized surface shape. The surface fitting errors were then analyzed in two ways: (i) a qualitative analysis by visual inspection that relies on the graphical representation of the point cloud and the encountered surface solution and (ii) a quantitative analysis based on the values of the surface fitting errors measured as the signed Euclidean distances and associated statistics.

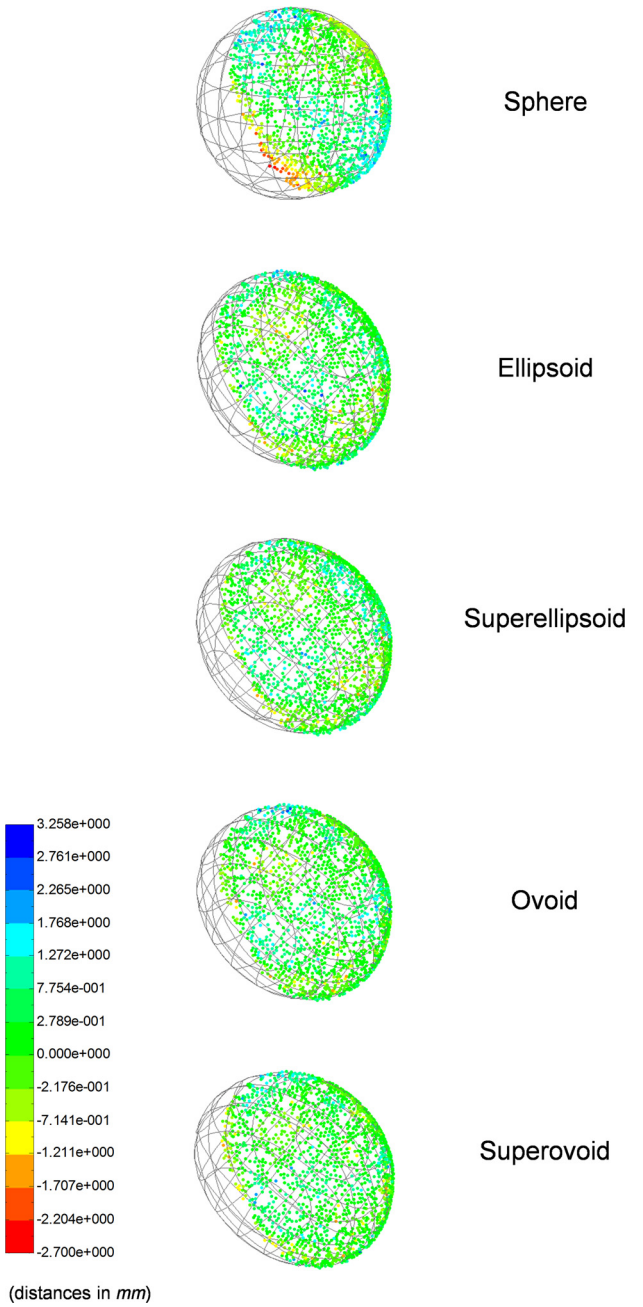

Fig. 3 Three-dimensional views of the optimally fitted surfaces of a femoral head illustrating that the geometric primitives fit the data in a global fashion. Data points are represented based on the minimal signed Euclidean distances (in millimeter) calculated between each point and the idealized geometric primitive.

3 Results

By visual inspection, all fitted shape models approximated quite well the global features of the articular surfaces of the femoral heads, although nonspherical shapes presented a better anatomical fit (Fig. 3). From this qualitative analysis, it is also clear that the spherical shape have more concentrated areas of points with greater fitting errors relative to the remaining shapes.

Consistent with the qualitative analysis, the quantitative analysis of the surface fitting errors indicated that the bone–cartilage boundary of the femoral heads closely resembled the idealized geometric primitives, as the error metrics were very small (i.e., on the order of 10^{-1} mm). Tables 2 and 3 show the surface fitting errors and surface fitting parameters, respectively.

The mean fitting errors (Table 2) were smaller for the ovoid and superovoid shapes, where the largest difference of 0.159 mm lies between the sphere and ovoid. Both ellipsoid and superellipsoid mean fitting errors were similar, with the ellipsoid shape being 0.012 mm larger. The mean fitting errors between ovoid and superovoid were also very similar but 0.008 mm larger for the superovoid. The statistical analyses (paired t test) showed that the differences between fitting errors of the sphere and all other shapes were significant ($p < 0.05$). The ovoid and ellipsoid also presented a significant difference ($p = 0.011$). As for the differences between surface fitting errors for the 11 specimens of the ellipsoid and superellipsoid ($p = 0.069$), ellipsoid and superovoid ($p = 0.177$), superellipsoid and ovoid ($p = 0.402$), superellipsoid and superovoid ($p = 0.759$), and finally ovoid and superovoid ($p = 0.208$) were nonsignificant.

Table 1 Vector of shape parameters for the sphere (S), ellipsoid (E), superellipsoid (SE), ovoid (O), and superovoid (SO) shape models and corresponding number of geometric modeling degrees-of-freedom, *M*

Shape model	$\boldsymbol{\Lambda}$	*M*
S	$\boldsymbol{\lambda}_S = [a,t_1,t_2,t_3]^T$	4
E	$\boldsymbol{\lambda}_E = [a,b,c,t_1,t_2,t_3,\phi,\theta,\psi]^T$	9
SE	$\boldsymbol{\lambda}_{SE} = [a,b,c,\gamma_1,\gamma_2,\gamma_3,t_1,t_2,t_3,\phi,\theta,\psi]^T$	12
O	$\boldsymbol{\lambda}_O = [a,b,c,c_{0x},c_{1x},c_{2x},c_{3x},c_{0y},c_{1y},c_{2y},c_{3y},t_1,t_2,t_3,\phi,\theta,\psi]^T$	17
SO	$\boldsymbol{\lambda}_{SO} = [a,b,c,\gamma_1,\gamma_2,\gamma_3,c_{0x},c_{1x},c_{2x},c_{3x},c_{0y},c_{1y},c_{2y},c_{3y},t_1,t_2,t_3,\ \phi,\theta,\psi]^T$	20

Table 2 Surface fitting error statistics (in millimeter) for each geometric primitive for each femoral head. The total number of points (*N*) for each subject is also indicated. The mean (μ) and standard deviation (σ) are calculated for the absolute value of the surface error, $\|d_{PQ}\|_2$ (S—sphere; E—ellipsoid; SE—superellipsoid; O—ovoid; and SO—superovoid).

Subject	Gender	Age	Side	*N*		S	E	SE	O	SO
1	F	31	L	1265	μ	0.595	0.596	0.533	0.521	0.517
					σ	0.472	0.479	0.459	0.461	0.461
					Min	−2.51	−2.478	−2.555	−2.604	−2.088
					Max	-4.0×10^{-5}	2.220	2.056	2.275	2.358
2	M	28	R	1506	μ	0.580	0.584	0.569	0.527	0.535
					σ	0.508	0.500	0.518	0.494	0.489
					Min	−3.464	−2.616	−2.351	−2.469	−2.260
					Max	-2.0×10^{-5}	3.462	3.463	3.459	3.456
3	F	29	L	1085	μ	0.569	0.485	0.466	0.427	0.451
					σ	0.485	0.447	0.449	0.411	0.425
					Min	−2.770	−2.448	−2.249	−2.246	−2.218
					Max	-5.0×10^{-5}	2.176	2.279	1.962	2.357
4	M	24	L	1097	μ	0.811	0.744	0.731	0.593	0.606
					σ	0.603	0.564	0.557	0.543	0.552
					Min	−3.464	−2.573	−2.739	−2.442	−2.305
					Max	-3.0×10^{-5}	3.464	3.464	3.464	3.464
5	F	21	R	1145	μ	0.698	0.563	0.524	0.506	0.476
					σ	0.552	0.508	0.485	0.491	0.470
					Min	−3.461	−2.242	−2.445	−2.441	−2.544
					Max	-5.0×10^{-5}	3.462	3.459	3.463	3.463
6	F	21	R	1107	μ	0.602	0.429	0.451	0.423	0.425
					σ	0.517	0.420	0.438	0.426	0.418
					Min	−2.616	−2.122	−2.135	−2.558	−2.436
					Max	-6.0×10^{-5}	2.021	2.265	2.306	2.323
7	M	30	R	1106	μ	0.709	0.461	0.492	0.433	0.471
					σ	0.529	0.465	0.481	0.459	0.464
					Min	−2.723	−2.164	−2.365	−2.030	−2.226
					Max	-6.0×10^{-5}	2.274	2.131	2.254	2.204
8	M	32	L	1132	μ	0.704	0.647	0.640	0.585	0.603
					σ	0.508	0.493	0.474	0.488	0.519
					Min	−2.473	−2.604	−2.451	−2.230	−2.506
					Max	-4.0×10^{-5}	2.200	2.353	2.668	2.602
9	M	27	L	1065	μ	0.691	0.609	0.583	0.532	0.557
					σ	0.524	0.476	0.477	0.487	0.467
					Min	−3.451	−2.309	−2.899	−2.248	−2.094
					Max	-9.0×10^{-5}	3.463	3.319	3.455	3.428
10	F	21	R	1117	μ	0.821	0.515	0.528	0.470	0.495
					σ	0.494	0.439	0.447	0.433	0.436
					Min	−2.608	−2.315	−2.676	−2.008	−2.031
					Max	-1.1×10^{-4}	2.460	2.048	2.199	2.067
11	F	39	L	1759	μ	0.437	0.408	0.398	0.356	0.351
					σ	0.429	0.397	0.397	0.372	0.363
					Min	−2.003	−2.361	−2.229	−2.227	−2.084
					Max	2.376	1.932	1.997	2.011	1.969
Fitting error for all 11 specimens					μ	0.643	0.544	0.532	0.484	0.493
					σ	0.521	0.481	0.479	0.465	0.466
					Min	−3.463	−2.616	−2.899	−2.604	−2.544
					Max	2.376	3.464	3.464	3.463	3.464

Table 3 Shape parameters for each geometric primitive used to describe the femoral head. The values of a, b, c, t_1, t_2, and t_3 are in millimeter. Angular parameters are in radians (S—sphere; E—ellipsoid; SE—superellipsoid; O—ovoid; and SO—superovoid).

		S	E	SE	O	SO
a	$\mu \pm \sigma$	32.11 ± 4.66	32.37 ± 4.58	32.41 ± 4.57	33.10 ± 4.29	33.26 ± 4.06
	Range	21.62–37.22	21.36–37.28	21.38–37.54	23.33–38.15	23.33–37.38
b	$\mu \pm \sigma$	—	31.89 ± 4.88	31.67 ± 4.75	32.46 ± 4.69	33.03 ± 4.79
	Range		21.52–37.73	21.65–36.74	22.22–37.98	23.24–38.11
c	$\mu \pm \sigma$	—	31.79 ± 4.32	31.62 ± 4.40	31.79 ± 4.52	31.76 ± 4.36
	Range		21.88–36.76	21.01–36.29	20.93–36.61	21.39–36.70
γ_1	$\mu \pm \sigma$	—	—	2.05 ± 0.06	—	2.03 ± 0.04
	Range			2.00–2.18		2.00–2.09
γ_2	$\mu \pm \sigma$	—	—	2.03 ± 0.04	—	2.02 ± 0.03
	Range			2.00–2.12		2.00–2.09
γ_3	$\mu \pm \sigma$	—	—	2.04 ± 0.07	—	2.01 ± 0.03
	Range			2.00–2.17		2.00–2.09
c_{0x}	$\mu \pm \sigma$	—	—	—	0.97 ± 0.02	0.96 ± 0.04
	Range				0.93–0.99	0.87–0.99
c_{1x}	$\mu \pm \sigma$	—	—	—	0.03 ± 0.03	0.03 ± 0.03
	Range				2.48×10^{-5}–0.08	5.23×10^{-5}–0.09
c_{2x}	$\mu \pm \sigma$	—	—	—	0.01 ± 0.05	0.01 ± 0.06
	Range				−0.07 to 0.09	−0.09 to 0.09
c_{3x}	$\mu \pm \sigma$	—	—	—	0.04 ± 0.06	0.04 ± 0.05
	Range				−0.08 to 0.09	−0.06 to 0.09
c_{0y}	$\mu \pm \sigma$	—	—	—	0.98 ± 0.01	0.96 ± 0.02
	Range				0.97–0.99	0.92–0.99
c_{1y}	$\mu \pm \sigma$	—	—	—	0.01 ± 0.02	0.02 ± 0.01
	Range				9.95×10^{-6}–0.05	0.00–0.04
c_{2y}	$\mu \pm \sigma$	—	—	—	0.02 ± 0.03	0.02 ± 0.03
	Range				−0.04 to 0.06	−0.06 to 0.06
c_{3y}	$\mu \pm \sigma$	—	—	—	0.018 ± 0.06	0.04 ± 0.05
	Range				−0.07 to 0.09	−0.03 to 0.09
t_1	$\mu \pm \sigma$	224.72 ± 77.64	224.87 ± 77.53	224.89 ± 77.61	224.91 ± 77.58	224.85 ± 77.54
	Range	96.41–324.32	96.35–324.87	96.29–324.76	96.29–324.29	96.33–324.16
t_2	$\mu \pm \sigma$	0.29 ± 58.00	0.38 ± 58.09	0.22 ± 58.03	0.24 ± 57.87	0.30 ± 57.86
	Range	−168.14 to 41.57	−168.21 to 1.75	−168.11 to 41.99	−167.73 to 41.56	−167.62 to 41.61
t_3	$\mu \pm \sigma$	16.64 ± 40.57	16.81 ± 40.54	16.77 ± 40.56	16.74 ± 40.70	16.61 ± 40.58
	Range	−11.50 to 37.16	−11.39 to 37.19	−11.38 to 37.22	−11.16 to 37.68	−11.35 to 137.12
ϕ	$\mu \pm \sigma$	—	10.59 ± 3.42	10.02 ± 4.12	9.81 ± 4.75	10.02 ± 5.15
	Range		5.28–15.54	2.51–14.94	−0.67 to 15.51	−1.74 to 16.37
ϑ	$\mu \pm \sigma$	—	10.581 ± 4.20	10.85 ± 3.42	10.50 ± 4.39	10.59 ± 4.37
	Range		3.17–16.46	6.69–16.16	2.86–16.78	3.25–17.49
ψ	$\mu \pm \sigma$	—	10.65 ± 3.63	10.37 ± 3.77	9.95 ± 5.12	9.68 ± 5.61
	Range		6.79–16.36	6.26–15.63	−1.65 to 16.49	−3.47 to 16.09

As for the shape parameters, the mean surface dimensions were similar for the sphere, ellipsoid, and superellipsoid (largest difference is between superellipsoid and sphere: 0.299 mm), but were slightly larger for the ovoid and superovoid (largest difference is between superovoid and sphere: 1.149 mm). The dimensions also reveal that ellipsoids, superellipsoid, ovoid, and superovoid were more eccentric along the local x axis since the a value is greater than b and c for all these shapes. Interestingly, the exponent values of superellipsoid and superovoid were very close to 2.0 where the highest γ value, for all 11 subjects, was 2.179, hence, both super shapes were very similar to their quadratic counterparts. As for the centroid positions and surface orientations, all shapes showed very similar values.

4 Discussion

MacConaill's mathematical and clinical work on synovial joint morphology indicates that the macroscopic features of spheroidal articular surfaces closely follow an ovoidal form [17–19]. Although his classification has been known for over 40 years, many computer-aided orthopedic surgery methodologies still remain faithful to the spherical classification. On the other hand, several studies have considered nonspherical shapes but none were truly ovoidal [4–15]. Generic ovoidal shapes could contribute significantly to the anatomical description of human joints and to design improved artificial joints.

In this work, MacConaill's morphological classification is computationally tested. To this end, a set of 11 femoral head point clouds underwent a surface fitting procedure which considers spherical, ellipsoidal, superellipsoidal, ovoidal, and superovoidal shapes as geometric models that describe joint morphology. The developed surface fitting framework has the following capabilities: (i) is easily extendable to other (implicit) shape models; (ii) it accurately measures subject-specific morphofunctional parameters, such as articular centers, functional axes, and mechanical

axes; and (iii) it performs a best fit shape comparison based entirely on signed Euclidean distances between points and fitted surface rather than pseudo-Euclidean distances.

The surface fitting error results (Table 2) indicate that the femoral head is better described by ovoid shapes which have the lowest surface fitting errors, along with the lowest standard deviation, followed by the superovoid, superellipsoid, ellipsoid, and finally the sphere that presents the highest surface fitting error. Interestingly, the largest surface fitting error was between sphere and ovoid shapes, not between sphere and superovoid as initially expected. In particular, the fitting error of the ovoid was 24.75% less than the fitting error of the sphere. Thus, the ovoid describes the shape of the femoral head best, with the superovoidal shapes with exponents slightly greater than 2.0 having a poorer fit.

The main novelty of this work consists of introducing shapes with irrational-degree (i.e., $\gamma_i > 2.0$) and ovoidal features into morphological studies of the articular surface of the femoral head. Such shapes provide a higher degree of geometric modeling freedom relative to a sphere (i.e., a wider range of curvatures from round to squared forms and axial asymmetry). The results show that the ovoidal asymmetry contributes to the increased goodness-of-fit compared to nonovoidal shapes, thus corroborating MacConaill's classification.

One limitation of this work is that the approach was only tested on 11 data sets. A greater number of data sets would provide more statistical significance. Even so, the results validate MacConaill's observations and points toward new research paths on morpho-functional studies of other spheroidal articular surfaces, such as the acetabular cavity, humeral head, and glenoid cavity. Since this work introduces ovoidal shapes to represent the morphology of the femoral head, it is necessary to perform additional surface fitting tests with other ovoid shapes, such as the tapered (super)ellipsoid [20], in order to determine if there are more suitable shapes besides the ones considered. Another limitation is related to the computational framework, as the various image processing, mesh adjustment, and surface fitting operations should be integrated into a single stand-alone software if such computational tool is to be used in a clinical setting. In addition, the computational framework could be more efficient with the addition of parallel processing, as several of the surface fitting algorithms are performed in parallel.

The surface fitting framework and consequent findings have applications in the development of novel computer-aided orthopedic tools that consider ovoidal shapes in the diagnosis and treatment of hip joint disorders. In particular, the high precision control offered by the framework outputs geometric measurements for personalized anatomy, allowing for the fabrication of endoprosthesis with ovoidal shapes with subject-specific dimensions and curvatures.

Acknowledgment

The authors would like to acknowledge the financial support given by the Fundação para a Ciência e a Tecnologia (FCT) and by the UT Austin|Portugal Program. The first author would like to thank FCT for the Ph.D. Grant No. SFRH/BD/47750/2008. This work was also partially supported by national funds through FCT with reference UID/CEC/50021/2013.

Nomenclature

a = shape coefficient along the x_l direction
b = shape coefficient along the y_l direction
c = shape coefficient along the z_l direction
c_{0x} = ovoidal shape coefficient along the x_l direction
c_{1x} = ovoidal shape coefficient along the x_l direction
c_{2x} = ovoidal shape coefficient along the x_l direction
c_{3x} = ovoidal shape coefficient along the x_l direction
c_{0y} = ovoidal shape coefficient along the y_l direction
c_{1y} = ovoidal shape coefficient along the y_l direction
c_{2y} = ovoidal shape coefficient along the y_l direction
c_{3y} = ovoidal shape coefficient along the y_l direction
$\mathbf{D}$ = surface scaling matrix
$\mathbf{d}_{PQ}$ = distance vector between points P and Q
EOF = error-of-fit objective function
f = residual of error-of-fit objective function
F_{SO} = implicit surface expression for a superellipsoid
F_{SQ} = implicit surface expression for a superovoid
i = index for points
I_k = real-valued interval of the kth surface parameter
k = index for surface parameter
$\mathbf{l}$ = lower bound column vector
M = number of geometric modeling degrees-of-freedom
N = total number of points
$\mathbf{P}$ = set of N points in Cartesian space
$\mathbf{R}$ = surface orientation matrix
SED = signed Euclidean distance objective function
$\mathbf{t}$ = surface translation vector
$\mathbf{u}$ = upper bound column vector
$\mathbf{x}$ = position vector of a point
$\mathbf{x}_g$ = position vector of a point in global coordinates
x_l = local coordinates of a point in space along the x-direction
$\mathbf{x}_l$ = position vector of a point in local coordinates
$\mathbf{x}_P$ = position vector of given point from point cloud
$\mathbf{x}_Q$ = position vector of surface point with minimum distance
y_l = local coordinates of a point in space along the y-direction
z_l = local coordinates of a point in space along the z-direction
γ_1 = roundness exponent along the x_l direction
γ_2 = roundness exponent along the y_l direction
γ_3 = roundness exponent along the z_l direction
ε = tolerance scalar
$\boldsymbol{\varepsilon}$ = tolerance vector
$\boldsymbol{\lambda}$ = vector of surface geometric parameters
$\boldsymbol{\lambda}^*$ = vector of geometric parameters of the optimally fitted surface
υ = surface orientation angle with respect to the x-direction
φ = surface orientation angle with respect to the y-direction
ψ = surface orientation angle with respect to the z-direction
Ω = admissible set or surface parameter space
$\|.\|_2$ = Euclidean norm
$\mathbf{0}_{1x3}$ = zero row vector

References

[1] Netter, F. H., 2011, *Atlas of Human Anatomy. Professional Edition*, 5th ed., Elsevier, Saunders, Philadelphia, PA.
[2] Agur, A. M. R., and Dalley, A. F., 2012, *Grant's Atlas of Anatomy*, 13th ed., Lippincott Williams & Wilkins, Philadelphia, PA.
[3] Schuenke, M., Schulte, E., Schumacher, U., Ross, L. M., and Lamperti, E. D., 2012, *Atlas of Anatomy—General Anatomy and Musculoskeletal System*, 1st ed., Thieme, Stuttgart, Germany.
[4] Kang, M. J., Sadri, H., Stern, R., Magnenat-Thalmann, N., Hoffmeyer, P., and Ji, H. S., 2011, "Determining the Location of Hip Joint Centre: Application of a Conchoid's Shape to the Acetabular Cartilage Surface of Magnetic Resonance Images," Comput. Method Biomech. **14**(1), pp. 65–71.
[5] Cerveri, P., Marchente, M., Chemello, C., Confalonieri, N., Manzotti, A., and Baroni, G., 2011, "Advanced Computational Framework for the Automatic Analysis of the Acetabular Morphology From the Pelvic Bone Surface for Hip Arthroplasty Applications," Ann. Biomed. Eng., **39**(11), pp. 2791–2806.
[6] Anderson, A. E., Ellis, B. J., Maas, S. A., and Weiss, J. A., 2010, "Effects of Idealized Joint Geometry on Finite Element Predictions of Cartilage Contact Stresses in the Hip," J. Biomech., **43**(7), pp. 1351–1357.
[7] Xi, J., Hu, X., and Jin, Y., 2003, "Shape Analysis and Parameterized Modelling of Hip Joint," ASME J. Comput. Inf. Sci. Eng., **3**(3), pp. 260–265.
[8] Gu, D. Y., Chen, Y. Z., Dai, K. R., Zhang, S., and Yuan, J., 2008, "The Shape of the Acetabular Cartilage Surface: A Geometric Morphometric Study Using Three-Dimensional Scanning," Med. Eng. Phys., **30**(8), pp. 1024–1031.
[9] Allaire, S., Burdin, V., Jacq, J.-J., Moineau, G., Stindel, E., and Roux, C., 2007, "Robust Quadric Fitting and Mensuration Comparison in a Mapping Space Applied to 3D Morphological Characterization of Articular Surfaces," 4th IEEE International Symposium on Biomedical Imaging: From Nano to Macro (ISBI 2007), Arlington, VA, Apr. 12–15, pp. 972–975.
[10] Allaire, S., Jacq, J.-J., Burdin, V., and Roux, C., 2007, "Ellipsoid-Constrained Robust Fitting of Quadrics With Application to the 3D Morphological Characterization of Articular Surfaces," 29th Annual International Conference of the

IEEE Engineering in Medicine and Biology Society (EMBS 2007), Lyon, France, Aug. 22–26, pp. 5087–5090.
[11] Jacq, J.-J., Roux, C., Stindel, É., and Lefèvre, C., 2000, "Analytical Surface Recognition in Three-Dimensional (3D) Medical Images Using Genetic Matching: Application to the Extraction of Spheroidal Articular Surfaces in 3D Computed Tomography Data Sets," Int. J. Imaging Syst. Technol., **11**(1), pp. 30–43.
[12] Liu, B., Hua, S., Zhang, H., Liu, Z., Zhao, X., Zhang, B., and Yue, Z., 2014, "A Personalized Ellipsoid Modeling Method and Matching Error Analysis for the Artificial Femoral Head Design," Comput. Aided Des., **56**, pp. 88–103.
[13] Matsuura, Y., Ogihara, N., and Nakatsukasa, M., 2010, "A Method for Quantifying Articular Surface Morphology of Metacarpals Using Quadric Surface Approximation," Int. J. Primatol., **31**(2), pp. 263–274.
[14] Eckhoff, D. G., Bach, J. M., Spitzer, V. M., Reinig, K. D., Bagur, M. M., Baldini, T. H., Rubinstein, D., and Humphries, S., 2003, "Three-Dimensional Morphology and Kinematics of the Distal Part of the Femur Viewed in Virtual Reality: Part II," J. Bone Joint Surg. Am., **85**(S4), pp. 97–104.
[15] Menschik, F., 1997, "The Hip Joint as a Conchoids Shape," J. Biomech., **30**(9), pp. 971–973.
[16] Cerveri, P., Manzotti, A., and Baroni, G., 2014, "Patient Specific Acetabular Shape Modelling: Comparison Among Sphere, Ellipsoid and Conchoids Parameterisations," Comput. Method Biomech., **17**(5), pp. 560–567.
[17] MacConaill, M. A., 1966, "The Geometry and Algebra of Articular Kinematics," Biomed. Eng., **1**, pp. 205–212.
[18] MacConaill, M. A., 1973, "A Structuro-Functional Classification of Synovial Articular Units," Ir. J. Med. Sci., **142**(1), pp. 19–26.
[19] MacConaill, M. A., and Basmajian, J. V., 1977, *Muscles and Movements: A Basis for Human Kinesiology*, Krieger Publishing Company, Huntington, NY.
[20] Barr, A. H., 1981, "Superquadrics and Angle-Preserving Transformations," IEEE Comput. Graphics Appl., **1**(1), pp. 11–23.
[21] Todd, P. H., and Smart, I. H., 1984, "The Shape of Birds' Eggs," J. Theor. Biol., **106**(2), pp. 239–243.
[22] Yushkevich, P., and Gerig, G., 2014, "ITK-SNAP: Semi-Automatic Segmentation Using Active Contour Methods," accessed Apr. 10, 2015, http://www.itksnap.org/
[23] Kitware, 2015, "ParaView: Open-Source, Multi-Platform Data Analysis and Visualization Application," Kitware Inc., Clifton Park, NY, accessed Apr. 10, 2015, http://www.paraview.org/
[24] Blender Foundation, 2015, "Blender: Open Source 3D Content Creation Suite," Blender Foundation, Amsterdam, accessed Apr. 10, 2015, http://www.blender.org/
[25] MathWorks, 2015, "MATLAB: The Language of Technical Computing," The MathWorks Inc., Natick, MA, accessed Apr. 10, 2015, http://www.mathworks.com/products/matlab/
[26] Harris, M. D., Anderson, A. E., Henak, C. R., Ellis, B. J., Peters, C. L., and Weiss, J. A., 2012, "Finite Element Prediction of Cartilage Contact Stresses in Normal Human Hips," J. Orthop. Res., **30**(7), pp. 1133–1139.
[27] OsiriX: DICOM Viewer, 2014, "DICOM Sample Image Sets," Pixmeo, Geneva, Switzerland, accessed Apr. 10, 2015, http://www.osirix-viewer.com/datasets/
[28] Lorensen, W. E., and Cline, H. E., 1987, "Marching Cubes: A High Resolution 3D Surface Construction Algorithm," Comput. Graphics, **21**(4), pp. 163–169.
[29] LaValle, S. M., 2006, *Planning Algorithms*, Cambridge University Press, New York.
[30] Ribeiro, N. S., Fernandes, P. C. R., Lopes, D. S., Folgado, J., and Fernandes, P. R. A., 2009, "Solid and Finite Element Modeling of Biomechanical Structures: A Software Pipeline," 7th EUROMECH Solid Mechanics Conference, Lisbon, Portugal, Sept. 7–11.
[31] Lopes, D. S., 2013, "Smooth Convex Surfaces for Modeling and Simulating Multibody Systems With Compliant Contact Elements," Ph.D. thesis, Instituto Superior Técnico, Universidade de Lisboa, Lisbon, Portugal.